# Measurement and Modelling of Droplet Coalescence and Breakage in a Pulsed-Plate Extraction Column

Droplet coalescence and breakage rates in a pulsed-plate extraction column have been measured using the colorimetric method of Hamilton and Pratt (1980). The results were interpreted in terms of rate constants, defined appropriately for the mixer-settler and emulsion regions of operation respectively, using a discrete population balance model. It is shown that the resulting values of these constants can be used to predict accurately the steady-state droplet-size distribution and apparent coalescence rate. Computations for a typical extraction system indicated that the effect of polydispersivity on performance is surprisingly small for the pulsed plate column.

**M. O. GARG and H. R. C. PRATT**

**Department of Chemical Engineering, University of Melbourne, Parkville, Australia**

## SCOPE

Increasing interest is being shown in the use of pulsed perforated-plate extraction columns, especially for the reprocessing of spent nuclear reactor fuels. However, difficulties arise in their design and scale-up due to insufficient knowledge of the effects of axial dispersion of the continuous phase and of polydispersivity of the droplet phase on performance. These problems are compounded by the fact that the optimum performance occurs at a pulse energy input in the region of the transition between mixer-settler and emulsion type operation (Sege and Woodfield, 1954).

The present work is concerned with the effect of droplet coalescence and breakage on the steady-state droplet-size distribution, and on column performance, in both regions of operation. For this purpose the colorimetric method of Hamilton and Pratt (1980) was used to determine droplet coalescence and breakage rates.

## CONCLUSIONS AND SIGNIFICANCE

Coalescence rates were obtained for the methyl isobutyl ketone (MIBK)–water system in a 74-mm-diameter pulsed-plate column with typical plate geometry at three values of the pulse energy input, each at 3 to 4 values of the dispersed-phase holdup. The range of droplet sizes present was found to decrease with increasing pulsation rate due to a reduction in the upper size limit.

The results were interpreted by means of a discrete population balance model written for each of the droplet sizes present. The resulting equations, in matrix form, were solved for the second-order coalescence and first-order breakage rate constants, defined appropriately for the mixer-settler and emulsion regions of operation respectively. The rate constants thus obtained were correlated in terms of droplet size and holdup by expressions of the type

$$k_j \text{ or } K_j = a(d_j)^b(x_d)^c$$

It is shown that the rate constants can be used to predict accurately both the steady-state droplet-size distribution and the apparent coalescence rate. They were also used in a computer simulation to determine the effects of droplet coalescence and breakage on the effective rate of mass transfer for the system MIBK–acetic acid-water in a pulsed column. Although the results confirmed the beneficial effect of droplet interactions on performance, the extent was not significant due to the surprisingly small effect of polydispersivity itself. In consequence, there is little difference in the calculated number of plates required assuming a monodispersion of size equal to the Sauter mean diameter of the polydispersion, resulting in a valuable simplification for design purposes.

### INTRODUCTION

Experimental measurements of interdroplet coalescence rates are comparatively few in number and, with one important exception, are confined almost entirely to agitated vessels at low dispersed-phase holdup. Some work has also been reported on the theoretical modelling of droplet coalescence and breakage rates in terms of both continuous and discrete population balances; however, in attempting to apply these, e.g., to the prediction of the droplet-size distribution, assumed values of the parameters have been used in the absence of experimental values. A complete review of published work in these areas has been given by Hamilton and Pratt (1980, 1984).

The exception referred to above relates to the work of Hamilton and Pratt (1980, 1984), who used a novel colorimetric method to measure droplet coalescence rates in a packed liquid extraction column. This involved the size equilibration of separate streams of methyl isobutyl ketone droplets, containing respectively dithizone (green) and nickel di(ethyl xanthate) (yellow) in a section of packed column provided with longitudinal partitions. The droplets were then allowed to mingle and to enter a second, unpartitioned, column section, when coalescence of green and yellow droplets gave red droplets, the proportions of which were determined photographically. The present work is concerned with the application of the same technique to the pulsed perforated-plate column operating in both mixer-settler and emulsion regions.

M. O. Garg is presently with the Research and Development Dept., Engineers India Ltd., New Delhi, India. Correspondence concerning this paper should be addressed to H. R. C. Pratt.

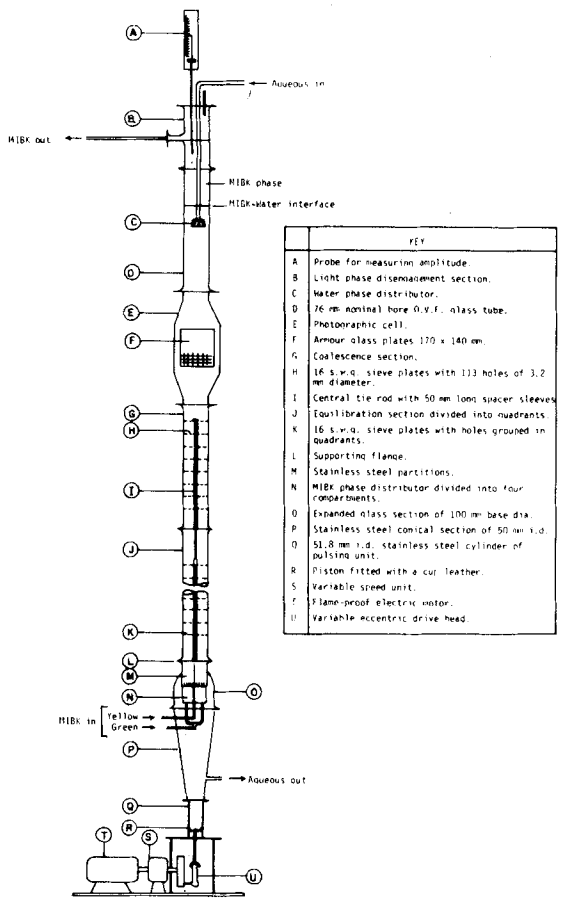


**Figure 1. Schematic diagram of pulsed column.**

## EXPERIMENTAL

### Preliminary Tests

Initially, the column design was based on that of the packed column described by Hamilton (1981); see also Hamilton and Pratt (1980, 1984). Thus it comprised a 72.45-mm-diameter vertically-partitioned droplet-size equilibration section surmounted successively by a photographic window, an unpartitioned coalescence section, a second window and an interface section. However, in operation it was found that large red droplets were formed by coalescence in the upper tapered section of the lower window and on the end of the central support rod for the plates. The lower window was, therefore, removed and the support for the plates modified; tests with no plates in the upper section then showed that no red droplets were formed.

During these tests it was also found that clear photographs of the finely dispersed droplets formed could not be obtained, especially at the highest pulse frequency, using the above workers' method. A modified method, using a macroscopic technique, was therefore adopted, as described later.

### Details of Final Equipment

The column is shown diagrammatically in Figure 1. The equilibration section comprised a 1.0-m-long precision bore glass tube of 72.45 mm inside diameter provided with 16 close-fitting sieve plates, made from 1.575 mm thick S.S. sheet, spaced 50 mm apart by means of a central tie rod and spacer sleeves. The plates were drilled with 113 holes of 3.2 mm diameter on an equilateral triangular pitch of 5 mm to give a free area of 21.7%; the holes were grouped into quadrants separated by at least 5 mm. Four longitudinal 1.0 mm thick S.S. partitions were soldered on each of the spacer sleeves, and their edges machined to fit the glass tube closely. The entire assembly was clamped together on the central tie rod, of 7.9 mm diameter, with the partitions located between the groups of holes.

The coalescence section consisted of a 0.5-m length of 76-mm-diameter nominal bore glass tube provided with from one to eight sieve plates. The latter, which were mounted on an extension of the tie rod supporting the plates in the equilibration section, were machined to fit the glass tube closely. The plate geometry was similar to that of those in the lower section, except that the holes were drilled on a uniform triangular pitch of 6 mm. The interface section was a 0.3-m-long section of 76-mm bore glass tube surmounted by an unequal pipe tee of the same diameter.

The photographic cell comprised a 1.22-mm-thick S.S. body with tapered ends and 220 mm × 180 mm parallel sides 28 mm apart. The latter were fitted with 170 mm × 140 mm armour glass windows, sealed with Teflon gaskets. Both windows were provided with millimeter scales, and the front one with a rectangular grid.

The bottom of the equilibration section terminated in an expanded glass section of 100 mm base diameter. This contained the solvent distributor, which consisted of a 40 mm length of 75 mm o.d. S.S. tube closed by a nozzle plate at the top and a cover containing the inlet pipes at the base. The body was divided into four compartments each provided with eleven 2.64 mm i.d. nozzles on the nozzle plate. Longitudinal partitions were provided between the nozzle plate and bottom sieve plate to prevent mixing of droplets from adjacent quadrants.

The expanded glass section was supported on a 1.22-mm-thick S.S. conical section with a base diameter of 50 mm. This in turn was supported on the pulsing unit, which comprised a piston fitted with a cup leather in a 51.8-mm i.d. S.S. cylinder. The piston was connected by a crank arm to a variable eccentric drive head giving a maximum stroke of 100 mm, corresponding to a pulse travel of 47 mm in the column. It was driven by a motor and variable speed drive providing a speed range of 0 to 360 cycles/min. The pulse height was determined at the air-water interface using a pointed probe with a transistor amplifier, 9-V battery and light emitting diode (LED). The amplitude corresponded to the difference in the probe positions which just gave intermittend and continuous glowing respectively of the LED.

The arrangement of the auxiliary equipment was similar to that used by Hamilton and Pratt (1980, 1984). Full details have been given by Garg (1982).

### Materials Used

Distilled water was used as continuous-phase and commercial-grade methyl isobutyl ketone as dispersed phase. Both phases were mutually saturated before use. The spent MIBK was recycled after passage through two 1.0-m-long sections of 100-mm-diameter glass column in series packed with I.C.I. "Darco" grade activated carbon, followed by a sand filter. No significant change was observed in the interfacial tension of the MIBK/water after regeneration of the MIBK, using a du Noüy balance.

The reagent concentrations used were 0.17 g/L for nickel di(ethyl xanthate) and 0.075 for dithizone; the former was in approximately three times the stoichiometric ratio. The dithizone was added to the MIBK immediately before a run in view of its instability.

### Procedure

The column was filled with aqueous feed and the pulse frequency was set. The aqueous feed was then set to the desired value, followed by the two MIBK flows, and the MIBK/water interface was maintained constant by adjustment of the needle valve on the exit aqueous stream. After stabilisation, requiring 10 to 15 minutes, four to five photographs of the window were taken on Kodak Ektachrome 35 mm professional color slide film with an effective speed of ASA160 under the tungsten light source used. Runs were conducted at ambient temperature, i.e., 20–23°C.

The camera had a 50-mm F1.8 standard lens mounted on a 25-mm extension tube, and was fitted with two close-up lens of 40-cm focal length; this gave a magnification of about 0.8 times the actual size with a minimum focussing distance (i.e., lens to front glass) of 7 cm. A shutter speed of 1/1,000 s was used with the $F$ stop selected to give the correct exposure. Illumination was provided by a 500 W tungsten lamp directly behind the photographic cell, from which it was separated by graphic art tracing paper.

The slides were projected on a white screen to give a magnification of about 40 times actual size. Around 1,000 droplets were counted for each set of conditions (200–250 per slide) within randomly selected grid areas, their diameters, or major and minor axes for oblate droplets, being recorded together with their colour. The actual sizes were obtained by relating the apparent size to that of the scale on the front window, and effective diameters of $d_e = (d_1^2 d_2)^{1/3}$ were calculated for the oblate droplets, where $d_1$ and $d_2$ are the major and minor axes respectively.

## RESULTS

Runs were carried out at pulse frequencies of 60, 90 and 120 cycles/min with a fixed pulse amplitude of 1.4 cm; for each fre-

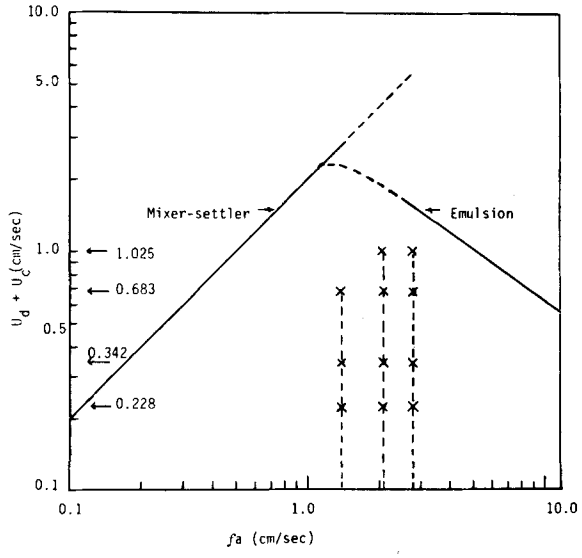


**Figure 2. Operating range in relation to flooding curves.**

TABLE 1. DETAILS OF SELECTED SIZE INTERVALS

| $j$ | Mean Diameter (mm) | Length of Size Interval: ≥ Lower Size Limit (mm) | Length of Size Interval: < Upper Size Limit (mm) |
|---|---|---|---|
| 1 | 0.3558 | 0.3149 | 0.3968 |
| 2 | 0.4483 | 0.3968 | 0.4999 |
| 3 | 0.5649 | 0.4999 | 0.6299 |
| 4 | 0.7117 | 0.6299 | 0.7936 |
| 5 | 0.8967 | 0.7936 | 0.9999 |
| 6 | 1.1297 | 0.9999 | 1.2598 |
| 7 | 1.4234 | 1.2598 | 1.5872 |
| 8 | 1.7933 | 1.5872 | 1.9997 |

TABLE 2. VARIATION OF DROPLET SIZE RANGE WITH PULSE FREQUENCY

| Pulse Frequency (cycles/min) | No. of Size Intervals M | Mean Dia. of First Interval (mm) | Mean Dia. of Last Interval (mm) |
|---|---|---|---|
| 60 | 8 | 0.3558 | 1.7933 |
| 90 | 7 | 0.3558 | 1.4234 |
| 120 | 6 | 0.3558 | 1.1297 |

quency, two, four and eight plates were used in the coalescence section, each with total throughput rates (continuous + dispersed) of 10, 15 and 30 cm$^3$/s and, at the two higher frequencies, 45 cm$^3$/s. Thus in all, 33 sets of runs were carried out, each with a MIBK/water volumetric flow ratio of unity.

From the appearance of the column during operation the runs at 60 and 120 cycles/min clearly corresponded to mixer-settler and emulsion operation respectively, while those at 90 cycles/min appeared to be in the transition region. This is confirmed by Figure 2, in which the flow rates are shown in relation to the flooding curves on the Sege-Woodfield diagram (1954); in this the limiting flows for the mixer-settler region are given by $U_c^f + U_d^f = 2fa$ and those for the emulsion region were calculated by the method of Thornton (1957).

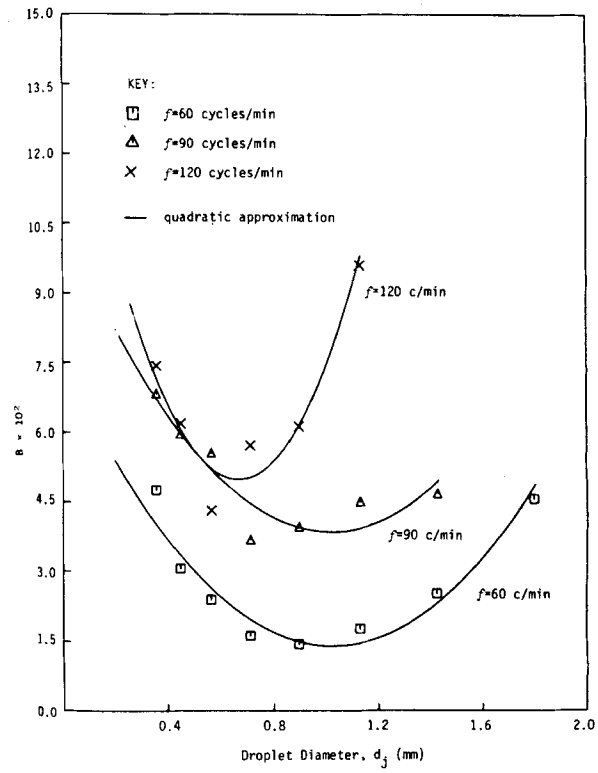


**Figure 3. Variation of constant $B$ in Eq. 1 with droplet diameter ($V_d + V_c$ = 30 cm$^3$/s).**

The droplets were grouped into size intervals such that the mean diameter in an interval was $2^{1/3}$ times that of the interval below. The selected intervals are given in Table 1, and the size range covered for each pulse frequency in Table 2.

To correct for scatter in the plots of fraction of red droplets of size $j$, i.e., $f_j$, vs. number of plates, $N$, the experimental data were fitted to an empirical expression satisfying the following conditions

(i) At $N = 0$: $f_j = 0$ and $\Delta f_j/\Delta N \neq 0$

(ii) As $N \to \infty$: $f_j \to 1.0$ and $\Delta f_j/\Delta N \to 0$

Statistical tests of the data by nonlinear regression, using Marquardt's algorithm (1963), were conducted with three expressions which satisfied these conditions. Of these, the following gave the best fit and reflected well the observed minimum in $f_j$ with increase in $d_j$ at each value of $N$ (Garg, 1982).

$$f_j = 1 - \exp(-NB) \tag{1}$$

The variation of the constant $B$ with $d_j$ in this equation was expressed satisfactorily by a second degree polynomial, giving the following expression for $f_j$

$$f_j = 1.0 - \exp[-N(b_1 + b_2 d_j + b_3 d_j^2)] \tag{2}$$

Equation 2 was finally fitted to the data by nonlinear regression analysis. The least squares estimates of $b_1$, $b_2$ and $b_3$ are given in Table 3, and a typical plot of $B$ vs. $d_j$ is shown in Figure 3. Plots of $f_j$ vs. $N$ for a total flow of 30 cm$^3$/s are shown in Figures 4 (a)-(c), which are included in supplementary material. The complete data are given by Garg (1982).

TABLE 3. ESTIMATES OF CONSTANTS IN EQ. 2

| $V_d + V_c$ cm$^3$/s | $f$ = 60 cycles/min: $b_1 \times 10^2$ | $b_2$ | $b_3 \times 10^2$ | $f$ = 90 cycles/min: $b_1 \times 10^2$ | $b_2$ | $b_3 \times 10^2$ | $f$ = 120 cycles/min: $b_1 \times 10^2$ | $b_2$ | $b_3 \times 10^2$ |
|---|---|---|---|---|---|---|---|---|---|
| 10 | 8.143 | −0.138 | 6.279 | 10.684 | −0.234 | 15.755 | 14.948 | −0.354 | 29.842 |
| 15 | 8.455 | −0.147 | 6.811 | 5.653 | −0.093 | 6.542 | 21.027 | −0.519 | 40.300 |
| 30 | 7.547 | −0.120 | 5.829 | 10.605 | −0.133 | 6.545 | 14.944 | −0.298 | 22.274 |
| 45 | — | — | — | 21.256 | −0.337 | 18.557 | 16.473 | −0.207 | 15.274 |

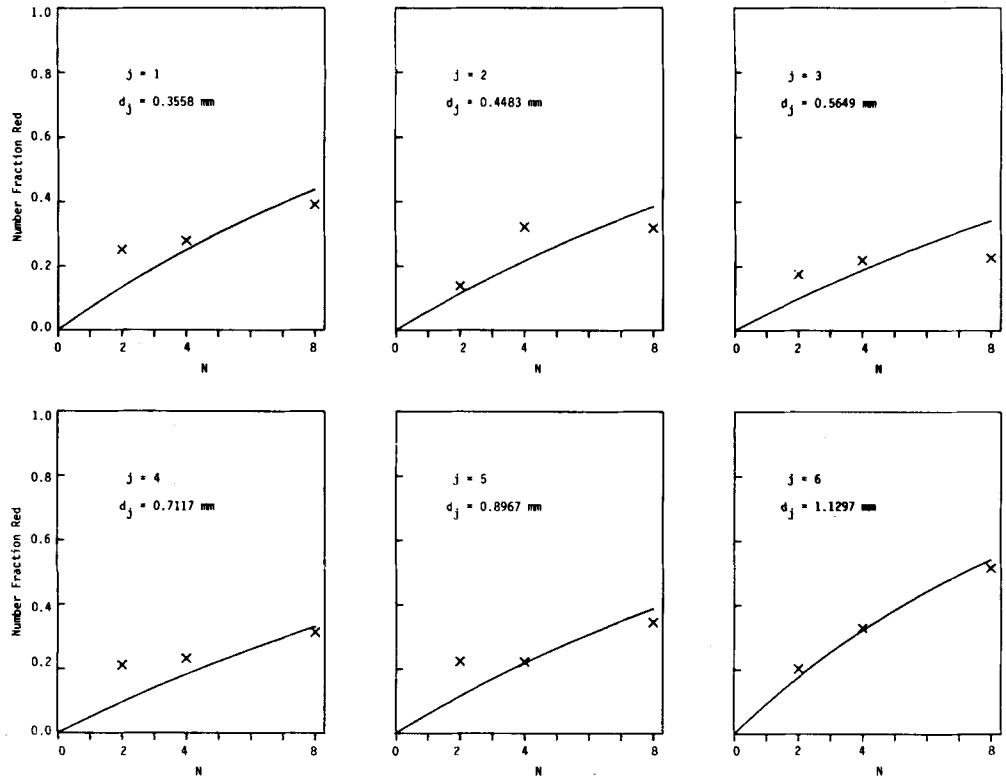


**Figure 4(c). Comparison of experimental values of $f_j$ with smoothed curves ($f$ = 120 cycles/min, $V_d + V_c$ = 30 cm³/s).**

## MODELLING OF DROPLET COALESCENCE AND BREAKAGE

### Basis of Method

The rates of coalescence and breakage of droplets can be related mathematically to the droplet-size distribution in terms of a discrete population balance model (Hamilton and Pratt, 1984) for the case of a packed column. Using this formulation, the coalescence and breakage fluxes are expressed as follows:

(i) Coalescences between equal-sized droplets of size $j$:

$$-\Delta n_j/\Delta t = 2k_j n_j^2 \tag{3}$$

(ii) Coalescences between unequal-sized droplets of sizes $j$ and $j-1$:

$$-\Delta n_j/\Delta t = k_j^{j-1} n_j n_{j-1} \tag{4}$$

(iii) Breakage of droplets of size $j$:

$$-\Delta n_j/\Delta t = K_j n_j \tag{5}$$

In Eqs. 3–5, $k_j$ and $k_j^{j-1}$ are second-order coalescence rate constants and $K_j$ are first-order breakage constants.

The dispersed phase in the present experiments consisted of yellow, green and red droplets, the latter being formed by coalescence of yellow and green droplets. Thus, two types of population balance are required: (i) over the total number of droplets in each size range entering and leaving a compartment (i.e., between two sieve plates); and (ii) over the number of red droplets in each size range entering and leaving a compartment in the coalescence section of the column.

The following assumptions are made in deriving the population balances.

(1) The individual processes of coalescence and breakage are mutually independent.

(2) In accordance with observation, the droplets undergo coalescence and breakage only on passage through the sieve plates, not within the compartments themselves.

(3) The droplet-size distribution is statistically homogeneous, i.e., there is no variation with position within the compartment.

(4) Breakage results in the formation of two equal-sized daughter droplets (Ramshaw and Thornton, 1967).

(5) The experimental droplet size distribution can be expressed in terms of discrete-size intervals, each an even multiple of the smallest droplet volume, $v_o$, present; thus

$$v_j = 2^j v_o, \text{ i.e., } d_j = 2^{j/3} d_o, \; j = 1,2,\cdots M$$

where $M$, the number of size intervals, varies with pulse frequency (Table 2). Hence coalescence of two droplets of size $j$ gives one of size $(j+1)$ and breakage of a droplet of size $j$ gives two of size $(j-1)$.

(6) Only coalescences between droplets in the same, and in adjacent size intervals are considered.

(7) In coalescences of droplets in adjacent size intervals $j$ and $(j-1)$, a fraction $p$ (generally taken as 0.5) of the droplets formed enter size $(j+1)$ and the remainder stay in size $j$.

(8) The rate constant $k_j^{j-1}$ for coalescence of droplets of adjacent sizes $j$ and $(j-1)$ can be approximated by

$$k_j^{j-1} = 0.5(k_j + k_{j-1}) \tag{6}$$

In accordance with assumption (2), the coalescence and breakage fluxes are expressed in terms of unit plate area, rather than unit free volume as for the packed column. Further, the number concentration, $n_j$, which appears as the driving force in the rate expressions, Eqs. 3–5, is defined for the mixer-settler region as the number of droplets of size $j$ per unit plate area, and for the emulsion region as the number per unit column volume.

### Droplet Number Concentrations

In the mixer-settler region the total droplet volume within a compartment is related to the dispersed-phase holdup, $x_d$, by

$$x_d = \sum_{i=1}^{M} n_i \pi d_i^3/6L \tag{7}$$

where subscript $i \equiv j$ and $n_i$ has dimensions of cm$^{-2}$. Solving for the number concentration of a specific size, $j$,

TABLE 4. FRACTIONAL HOLDUP OF DISPERSED PHASE

| Pulse Frequency (cycles/min) | Mode of Operation | $x_d$ at $V_d + V_c$ (cm³/s) of 10 | 15 | 30 | 45 |
|---|---|---|---|---|---|
| 60 | Mixer-Settler | 0.0224 | 0.0336 | 0.0673 | — |
| 90 | Mixer-Settler | 0.0149 | 0.0224 | 0.0448 | 0.0673 |
| 90 | Emulsion | 0.0187 | 0.0286 | 0.0612 | 0.0997 |
| 120 | Emulsion | 0.0232 | 0.0357 | 0.0780 | 0.1319 |

$$n_j = \frac{6x_d L}{\pi \sum_{i=1}^{M} n_i d_i^3/n_j} \qquad j = 1,2,\cdots,M \tag{8}$$

The ratios $n_i/n_j$ in Eq. 8 are obtainable from the experimental droplet-size distribution data. For the emulsion region the expression corresponding to Eq. 8 is

$$n_j = \frac{6x_d}{\pi \sum_{i=1}^{M} n_i d_i^3/n_j} \tag{9}$$

where $n_i$ now has dimensions of $cm^{-3}$.

The value of the holdup, $x_d$, for the mixer-settler region was obtained by equating the dispersed-phase volumetric flow to the volume of this phase transported by the pulse per unit time, giving

$$x_d = U_d/L\phi \tag{10}$$

The values for the emulsion region were calculated from the usual slip velocity equation using Thornton's correlation (1957) of the characteristic droplet velocity. The results are summarized in Table 4; in view of the uncertainty of the mode of operation at the frequency of 90 cycles/min, the holdup for this case was calculated for both modes.

#### Population Balances

The population balance equations were derived by a similar method to that used by Hamilton and Pratt (1984). The resulting equations were as follows:

(i) Total droplet population balance

$$\begin{aligned}\Delta_j = {} & k_{j-2}(0.5pn_{j-1}n_{j-2}) + k_{j-1}\{n_{j-1}^2 + 0.5pn_{j-1}(n_{j-2} \\ & - n_j)\} + k_j\{-n_j(2n_j + 0.5pn_{j-1} + 0.5n_{j+1})\} \\ & + k_{j+1}(-0.5n_jn_{j+1}) + K_j(-n_j) + K_{j+1}(2n_{j+1})\end{aligned} \tag{11}$$

where $\Delta_j = s\Delta n_j/\Delta N$ with $s = \phi$ for the mixer-settler region and $U_d/x_d$ for the emulsion region. The latter relation is derived on the assumption that the velocities of all droplet sizes within swarms tend to equalize, as in the sedimentation of solid particles.

(ii) Red droplet balance

$$\begin{aligned}\Delta_j^R = {} & k_{j-2}\{0.25pn_{j-1}n_{j-2}(1 + f_{j-1} + f_{j-2} - f_{j-1}f_{j-2})\} \\ & + k_{j-1}\{0.5n_{j-1}^2(1 + f_{j-1}^2) + 0.25pn_{j-1}n_{j-2}(1 + f_{j-1} \\ & + f_{j-2} - f_{j-1}f_{j-2}) + n_jn_{j-1}[0.25(1-p)(1+f_{j-1})(1-f_j) \\ & - 0.5pf_j]\} + k_j\{n_jn_{j-1}[0.25(1-p)(1+f_{j-1})(1-f_j) \\ & - 0.5pf_j] - n_j^2f_j(1+f_j) - 0.5n_jn_{j+1}f_j\} \\ & + k_{j+1}(-0.5n_jn_{j+1}f_j) + K_j(-n_jf_j) \\ & + K_{j+1}(2n_{j+1}f_{j+1})\end{aligned} \tag{12}$$

where

$$\Delta_j^R = s\Delta(n_jf_j)/\Delta N.$$

Equations 11 and 12 are derived assuming that, for droplets of size $j$, size intervals $(j-2)$, $(j-1)$ and $(j+1)$ each contain a significant number of droplets. However, this is not necessarily the case for the intervals at each end of the size distribution, and in fact the experimental data indicated that, although the numbers of droplets in size intervals 0 and $M+1$ were small in all cases, they could not be disregarded in the total droplet balance. Consequently, Eq. 11 was written also for these intervals, subject to the following conditions.

(i) Interactions involving droplets of size below 0 or above $M+1$ are not allowed, i.e., $n_j = 0$ for $j < 0$ or $> M+1$.

(ii) The breakage rate constant for size 0 is zero, i.e., $K_o = 0$.

(iii) The coalescence rate constant for size $M+1$ is zero, i.e., $k_{M+1} = 0$.

The droplet number balances, Eq. 11, are, therefore, written for $M+2$ size intervals (sizes 0 to $M+1$ inclusive), while the red droplet balances, Eq. 12, are written for $M$ size intervals (sizes 1 to $M$ inclusive); the latter applies since the data show that the values of $f_j$ for droplet sizes 0 and $M+1$ are too small to be meaningful. The resulting $2M+2$ equations are linear in the $k_j$ and $K_j$, and can therefore be expressed in matrix form as follows:

$$\boldsymbol{Ck} + \boldsymbol{BK} = \boldsymbol{\Delta} \tag{13}$$

$$\boldsymbol{C}^R\boldsymbol{k} + \boldsymbol{B}^R\boldsymbol{K} = \boldsymbol{\Delta}^R \tag{14}$$

where $\boldsymbol{C}$ and $\boldsymbol{C}^R$ are quadridiagonal matrices of the coefficients of the coalescence rate constants in Eq. 11 and 12 respectively, $\boldsymbol{B}$ and $\boldsymbol{B}^R$ are bidiagonal matrices of the coefficients of the breakage rate constants, and $\boldsymbol{k}$, $\boldsymbol{K}$, $\boldsymbol{\Delta}$ and $\boldsymbol{\Delta}^R$ are column vectors of the corresponding quantities in Eqs. 11 and 12.

Equation 13 and 14 can be further condensed as a simple partitioned matrix equation, as follows:

where

$$\boldsymbol{Ax} = \boldsymbol{z} \tag{15}$$

$$\boldsymbol{A} = \left[\begin{array}{c|c} \boldsymbol{C} & \boldsymbol{B} \\ \hline \boldsymbol{C}^R & \boldsymbol{B}^R \end{array}\right]$$

$$\boldsymbol{x} = [\boldsymbol{k} \mid \boldsymbol{K}]^T$$

$$\boldsymbol{z} = [\boldsymbol{\Delta} \mid \boldsymbol{\Delta}^R]^T$$

#### Solution of Population Balance Equations

A statistical analysis of the experimental data showed that the size distribution remained constant within the coalescence section of the column (Garg, 1982), so that $\boldsymbol{\Delta} = \boldsymbol{0}$; in addition, the elements of $\boldsymbol{\Delta}^R$ can be simplified to $sn_j\Delta f_j/\Delta N$. To obtain the true coalescence rates, i.e., with only green and yellow droplets present, the gradients $\Delta f_j/\Delta N$ were evaluated from the smoothed plots of $f_j$ vs. $N$ over the range of $N = 0$ to $N = 1$. The vector $\boldsymbol{z}$ therefore becomes

$$\boldsymbol{z} = [\boldsymbol{0} \mid \boldsymbol{\Delta}_{01}^R] \tag{16}$$

In principle, Eq. 15 can be solved directly by inversion of matrix $\boldsymbol{A}$. However, this was found not to be possible for $p = 0.50$, since then $\boldsymbol{A}$ is singular and does not have an inverse. A study of Eqs. 11 and 12 revealed that this is because the equations for the total droplet balance are linearly dependent in the form

$$\sum_{i=1}^{M+2} 2^{(i-1)}a_{i,j} = 0 \qquad j = 1,2,\cdots,2M+2 \tag{17}$$

where $a_{i,j}$ is the element in the $i$th row and $j$th column of $\boldsymbol{A}$. Solutions obtained with values of $p$ of 0.4, 0.6 and 0.75 showed that the rate constants do not vary greatly with $p$ and are close to those given in Tables 5(a)–(d) apart from the coalescence constants for the last size interval, i.e., $M$, which were always negative. [Tables 5(a)–(c) are included in supplementary material.]

Using the preferred value of $p$ of 0.5, it is clear that Eq. 15 constitutes an underdetermined set of equations which may not possess a unique solution. The solution can, however, be formulated as an optimization problem, the solution of which is the vector $\boldsymbol{x}$ which minimizes the residual vector, i.e.,

$$\epsilon = \boldsymbol{Ax} - \boldsymbol{z} \tag{18}$$

in terms of an appropriate norm. Two norms, i.e.,

$$\|\epsilon\|_1 = \sum_{i=1}^{2M+2} |\epsilon_i| \qquad (l_1 - \text{norm}) \tag{19}$$

TABLE 5(d). VALUES OF RATE CONSTANTS OBTAINED BY NEWTON-$l_1$ NORM METHOD. FREQUENCY = 120 cycles/min (EMULSION OPERATION)

| $j$ | Mean Dia. (mm) | Coalescence Constants, $k_j, L^4T^{-1}$ | | | | Breakage Constants, $K_j, LT^{-1}$ | | | |
|---|---|---|---|---|---|---|---|---|---|
| | | $V_d + V_c$ = 10 cm$^3$/s | $V_d + V_c$ = 15 cm$^3$/s | $V_d + V_c$ = 30 cm$^3$/s | $V_d + C_c$ = 45 cm$^3$/s | $V_d + V_c$ = 10 cm$^3$/s | $V_d + V_c$ = 15 cm$^3$/s | $V_d + V_c$ = 30 cm$^3$/s | $V_d + V_c$ = 45 cm$^3$/s |
| 1 | 0.3558 | $9.7191 \times 10^{-2}$ | $4.9447 \times 10^{-2}$ | $2.6254 \times 10^{-2}$ | $2.8827 \times 10^{-2}$ | 0.59979 | 0.77238 | 0.64146 | 0.82577 |
| 2 | 0.4483 | $2.5575 \times 10^{-2}$ | $2.6056 \times 10^{-2}$ | $2.8237 \times 10^{-2}$ | $2.3119 \times 10^{-2}$ | 0.48241 | 0.55075 | 0.49998 | 0.70740 |
| 3 | 0.5649 | $1.3471 \times 10^{-2}$ | $4.9135 \times 10^{-3}$ | $4.3411 \times 10^{-3}$ | $1.0038 \times 10^{-2}$ | 0.40658 | 0.42612 | 0.44591 | 0.67527 |
| 4 | 0.7117 | $5.3984 \times 10^{-3}$ | $4.4128 \times 10^{-3}$ | $3.0177 \times 10^{-3}$ | $2.8030 \times 10^{-3}$ | 0.43683 | 0.37753 | 0.40383 | 0.69546 |
| 5 | 0.8967 | $7.6093 \times 10^{-3}$ | $4.3055 \times 10^{-3}$ | $2.9017 \times 10^{-3}$ | $3.0106 \times 10^{-3}$ | 0.65420 | 0.60090 | 0.48498 | 0.71934 |
| 6 | 1.1297 | $5.5017 \times 10^{-7}$ | $9.5143 \times 10^{-7}$ | $7.3083 \times 10^{-7}$ | $2.7869 \times 10^{-7}$ | 1.46610 | 1.53660 | 0.92560 | 1.07990 |

$$\|\epsilon\|_2 = (\epsilon^T\epsilon)^{1/2} \qquad (l_2 - \text{norm}) \tag{20}$$

are commonly used because they offer more meaningful interpretation than other norms belonging to this class of $l_p$ ($0 < p < \infty$) norms (Rice, 1964).

*Solutions Based on $l_1$ Norm.* The $l_1$ approximation to $x$ is that which minimises the sum of $|\epsilon_i|$. Substituting Eq. 18 into Eq. 19, the objective function minimized is

$$\phi_1 = \sum_{i=1}^{2M+2} \left| \sum_{j=1}^{2M+2} a_{i,j}x_j - z_i \right| \tag{21}$$

Since $\phi_1$ is linear in the rate constants, i.e., the $x_j$'s, the minimization is most efficiently done by linear programming, using e.g., the algorithm developed by Barrodale and Roberts (1973, 1974). Using this algorithm, the rate constants were calculated for all operating conditions. The results were in good agreement with those in Tables 5(a)–(d), again apart from the coalescence constants for size $M$, which were always negative. This was apparently due to truncation of the size distribution to $M$ intervals.

The imposition of a lower bound, $x_j \geq 0$, for all values of $j$ was not possible with the above algorithm and an alternative method was therefore used. This involved conversion of the present optimisation problem with nonnegativity constraints into an unconstrained optimization by setting $x_j = y_j^2$ (Curtis, 1976). Thus the solution is obtained in terms of $y_j$, yielding positive values of $x_j$. Substituting this into Eq. 15, noting that $Ax - z = F(y)$, gives

$$F(y) = 0 \tag{22}$$

where

$$F_i(y) = \sum_{j=1}^{2M+2} a_{i,j}y_j^2 - z_i, \; i = 1, \cdots, 2M+2 \tag{23}$$

This system of nonlinear equations can be solved by Newton's method (Carnahan et al., 1969). Thus, an initial guess $y^o$ of $y$ is modified by a correction vector $\delta^k$, as follows

$$y^{k+1} = y^k + \delta^k \tag{24}$$

where $k$ is the iteration number. The correction vector is obtained by solving the following set of simultaneous linear equations

$$J^k\delta^k = -F(y^k) \tag{25}$$

where for the present case the Jacobian matrix is obtained from Eq. 23 as

$$J^k = 2AY^k \tag{26}$$

where $Y^k = \text{diag}\,(y_1^k, y_2^k, \cdots, y_{2M+2}^k)$. Since $A$ is singular for $p = 0.5$, $J^k$ is also singular and $\delta$ therefore cannot be obtained from Eq. 25 by matrix inversion. However, an $l_1$ approximation to $\delta$ can be computed by minimizing $\phi_1^k$, given by

$$\phi_1^k = \sum_{i=1}^{2M+2} \left| \sum_j J_{i,j}^k\delta_j^k + F_i(y^k) \right| \tag{27}$$

The algorithm of Barrodale and Roberts (1974) was used to minimize $\phi_1^k$ and the procedure was repeated until $|\delta_j^k| < 10^{-8}|y_j^{k+1}|$, $1 \leq j \leq 2M+1$. The rate constants were then obtained from the relations $x_j = y_j^2$. The values obtained by this method, termed the Newton – $l_1$ method, are given in Tables 5(a)–(d), in which the data for a pulse frequency of 90 cycles/min are interpreted on both mixer-settler and emulsion bases.

*Solution Using $l_2$ Norm.* Substitution of the error vector given by Eq. 18 into Eq. 20 and simplifying gives

$$\phi_2 = \|\epsilon\|_2^2 = x^TA^TAx - 2z^TAx + z^Tz \tag{28}$$

The objective function, $\phi_2$, is quadratic in $x$ and the latter can, therefore, be obtained by quadratic programming, subject to the lower bound, $x_j \geq 0$. Two algorithms for this purpose, *viz.*, Wolfe's and Beale's, both described by Van De Panne (1975), were available in the Multi-Purpose Optimization System (MPOS) on the Melbourne University computing system and were used to minimize $\phi_2$. Beale's method, which has a lower memory requirement, was used in the first instance and in the few cases where it failed to converge Wolfe's method was used. The results were essentially similar to those obtained by the Newton-$l_1$ norm method given in Tables 5(a)–(d); however, the latter method is preferred due to its more reliable convergence.

### Correlation of Rate Coefficients

The data in Tables 5(a)–(d) indicate that the rate coefficients vary with both droplet diameter and total throughput at all frequencies. They were therefore fitted by expressions of the type

$$k_j \text{ or } K_j = a(d_j)^b(x_d)^c \tag{29}$$

where the holdup, $x_d$, accounts for the effect of throughput.

The fitting was done by linear regression, giving values of the multiple regression coefficient, $R^2$, in excess of 77% in all cases. The resulting estimates of the constants $a$, $b$ and $c$ are summarized in Table 6. Since the rate constants are defined differently for mixer-settler and emulsion operation it was not possible to include the effect of pulse frequency. The data for 120 cycles/min are compared with the results of the regressions in Figure 5; those for the other frequencies are shown in Figures 6(a)–(c) and 7(a)–(c), which are included in supplementary material.

TABLE 6. REGRESSION VALUES OF COEFFICIENTS IN EQ. 29*

| $f$, cycles per min | Region of Operation | Values for $k_j$ | | | Values for $K_j$ | | |
|---|---|---|---|---|---|---|---|
| | | $a \times 10^4$ | $b$ | $c$ | $a$ | $b$ | $c$ |
| 60 | Mixer-Settler | 1.619 | −3.004 | −0.262 | 0.0715 | −1.113 | 0.328 |
| 90 | Mixer-Settler | 6.481 | −2.634 | 0.093 | 1.306 | −0.490 | 0.756 |
| 90 | Emulsion | 48.563 | −2.617 | −0.107 | 2.293 | −0.487 | 0.582 |
| 120 | Emulsion | 7.115 | −2.875 | −0.359 | 0.782 | −0.202 | 0.157 |

* Based on $d_j$ in mm, $k_j$ and $K_j$ in cm-s units.

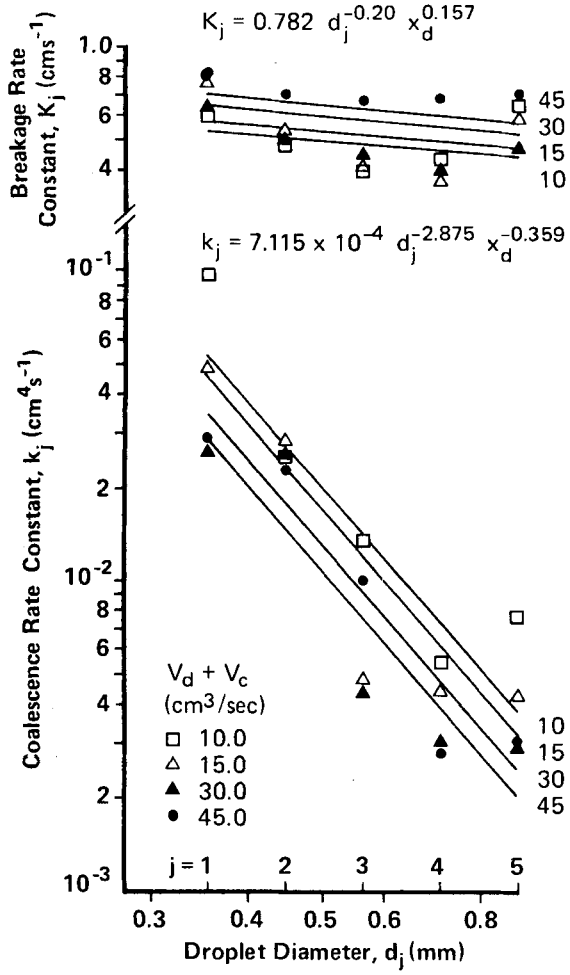


**Figure 5. Comparison of rate constants with values given by Eq. 29 ($f = 120$ cycles/min).**

## APPLICATIONS OF RATE CONSTANTS TO DESIGN

### Prediction of Steady-State Droplet-Size Distribution

A knowledge of the droplet-size distribution is of importance in design; it is, therefore, of interest to compare the distribution predicted by the model with the experimental distribution. A deterministic method can be used for this purpose with the present column type, using the following rearranged form of the relation defining $\Delta_j$:

$$n_{j,n} = n_{j,n-1} + \Delta_j/s \tag{30}$$

Thus, starting from the known inlet values of $n_j$, i.e., $n_{j,o}$, Eq. 30 is used recursively, together with Eq. 11 and the known rate constants, until the difference in the $n_j$ on two successive plates is negligible.

Typical results, starting from monosized inlet droplets, are shown in Figs. 8(a)–(c), (Figs. 8(a) and 8(c) are included in supplementary material.) A comparison of the predicted and experimental Sauter mean diameters is given in Table 7; this shows that agreement is very close. Calculations by the stochastic method described by Hamilton and Pratt (1984), using a Monte Carlo random selection technique, gave virtually identical results.

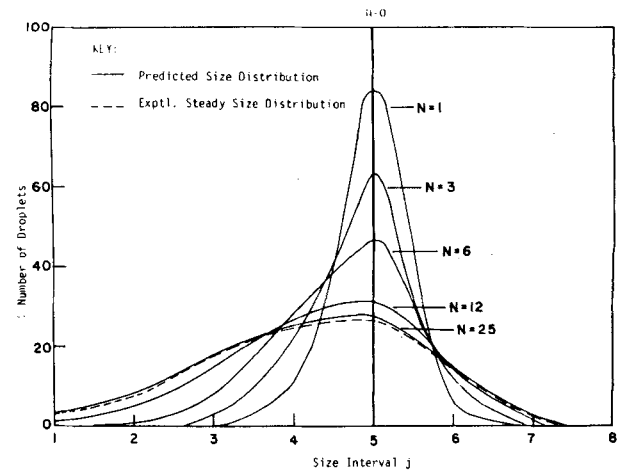


**Figure 8(b). Comparison of predicted and experimental droplet-size distribution ($f = 90$ cycles/min, $V_d + V_c = 15$ $cm^3/s$).**

### Prediction of Droplet Coalescence Rates

It is of interest to calculate the rate of red droplet formation, based on a steady-state size distribution, from the rate constants for comparison with the experimental values. Again using a deterministic method, the increase in $f_j$ over plate $n$ is obtained by arrangement of the relation defining $\Delta_j^R$, as follows

$$n_j f_{j,n} = n_j f_{j,n-1} + \Delta_j^R(f_n)/s \tag{31}$$

where $f_n$ is the column vector of $f_j$ values on plate $n$ and $\Delta_j^R(f_n)$, which denotes the functional dependence of $\Delta_j^R$ on $f_n$, is given by Eq. 12.

For any plate $n$, Eq. 31 represents a set of $M$ simultaneous nonlinear equations, which were solved for the $M$ unknown $f_{j,n}$ by an analogue of Newton's method in which the Jacobian matrix is replaced by a finite difference quotient approximation. The computations were carried out using steady state values of the $n_j$ calculated as described above; they were started from the first plate, with $f_o$ set to zero, and continued for eight plates.

The results are shown in Figures 9(a)–(c) in which values of $f_j$ calculated using both the smoothed and the actual values of the rate constants are compared with the experimental values. [Figures 9(a)–(b) are included in supplementary material.] This shows that agreement was good for the first few plates but that, as expected, the predicted values deviated upwards as $N$ increased due to the increasing incidence of multiple coalescences (i.e., red droplets with yellow or green), which become difficult to detect experimentally.

### Effect of Droplet Interactions on Mass Transfer

The effects of polydispersivity, and of droplet coalescence and

TABLE 7. COMPARISON OF PREDICTED WITH EXPERIMENTAL STEADY-STATE SAUTER MEAN DIAMETERS

| $V_c + V_d$ $cm^3 s^{-1}$ | 60 cycles/min Predicted $d_{32}$† (i) | 60 cycles/min Predicted $d_{32}$† (ii) | 60 cycles/min Expt'l $d_{32}$ | 90 cycles/min* Predicted $d_{32}$† (i) | 90 cycles/min* Predicted $d_{32}$† (ii) | 90 cycles/min* Expt'l $d_{32}$ | 120 cycles/min Predicted $d_{32}$† (i) | 120 cycles/min Predicted $d_{32}$† (ii) | 120 cycles/min Expt'l $d_{32}$ |
|---|---|---|---|---|---|---|---|---|---|
| 10.0 | 1.290 | 1.271 | 1.284 | 0.988 | 0.961 | 0.960 | 0.790 | 0.783 | 0.786 |
| 15.0 | 1.311 | 1.286 | 1.291 | 1.023 | 0.938 | 0.941 | 0.813 | 0.785 | 0.789 |
| 30.0 | 1.388 | 1.428 | 1.436 | 1.086 | 1.104 | 1.141 | 0.885 | 0.877 | 0.879 |
| 45.0 | — | — | — | 1.093 | 1.115 | 1.119 | 0.912 | 0.918 | 0.923 |

* Based on emulsion region of operation.
† Based on $k_j, K_j$ values (i) calculated from Eq. 29, (ii) from Tables 5(a)–(d).

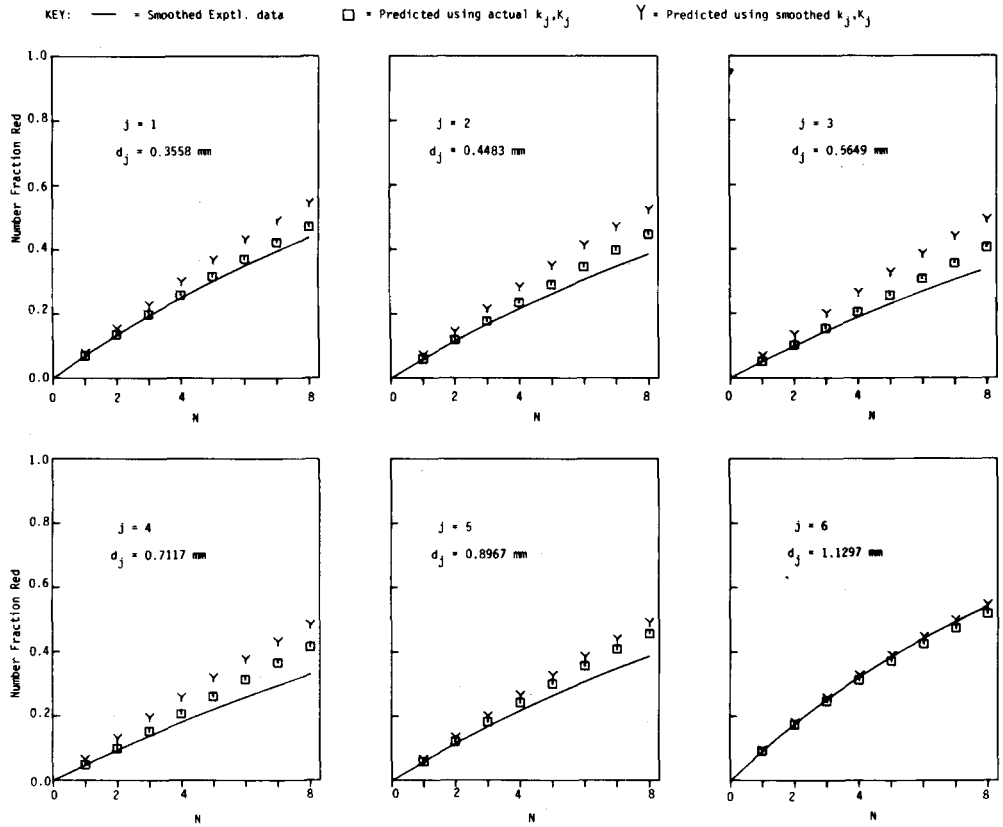


**Figure 9(c). Comparison of predicted and experimental fraction red curves ($f$ = 120 cycles/min, $V_d + V_c$ = 30 cm³/s).**

breakage, on the performance of a pulsed plate column of the present type was investigated theoretically for the extraction of 5% w/v aqueous acetic acid with MIBK to give a raffinate containing 0.1% of acetic acid. The column geometry was assumed identical with that used in the present experimental study, with the same pulse amplitude and frequencies. The holdup, $x_d$, and the extraction factor, $E = U_c/mU_d$, were assumed to be 0.132 and 0.70 respectively. The values of m, obtained from the equilibrium data of Vermijs and Kramers (1954) was 0.5449, and the calculated values of $U_d$ corresponding to $x_d$ were 0.670, 0.687 and 0.559 cm·s$^{-1}$ for the pulse frequencies of 60, 90 and 120 cycles/min respectively.

A modified form of backflow model was assumed in which only the continuous phase was fully mixed within stages. In consequence, the solute concentration in each droplet leaving a stage could be calculated analytically as follows,

$$c_{dj,n} = c^*_{d,n} - (c^*_{d,n} - c_{dj,n-1}) \exp\left[\frac{-6K_{od,j}L}{d_j v_{r,j}}\right] \tag{32}$$

Two cases were considered, *viz.*: (i) plug flow and (ii) backmixing of continuous phase; the backmixing ratios, $\alpha_c$, for the latter case were estimated as 1.5 for $f$ = 60 (Rouyer et al., 1974) and 4.8 and 5.0 for $f$ = 90 and 120 respectively (Garg and Pratt, 1981).

Mass transfer coefficients were calculated for each droplet size using the relation of Rozen and Bezzubova (1968) for "medium sized droplets" for the droplet phase; those for the continuous phase were obtained from Griffith's (1960) formula No.1 for $Re_d < 50$, and by Thorsen and Terjesen's correlation (1962) for larger droplets. The values of $K_{od}$ were then calculated for each size by means of the usual "two resistance" relation.

The computational procedure used was similar to that described by Hamilton and Pratt (1984) for the packed column, using height intervals corresponding to actual plates. It differed, however, in that Eq. B.1, in step 4, was replaced by Eq. 32, and Eqs. B.2 and B.3 for the backmixed case in step 5, were replaced by the following

$$C_{c,n+1} = C_{c,\text{out}} - \frac{U_d}{U_c}(c_{d,\text{in}} - \bar{c}_{d,n}) \tag{33}$$

where

$$C_{c,n+1} = (1 + \alpha_c)c_{c,n+1} - \alpha_c c_{c,n} \tag{34}$$

The computation started from the dispersed-phase inlet end using 2,000 droplets with their solute concentrations, initialized to zero at the inlet, each stored in a separate memory location; the latter were grouped into intervals according to the steady-state size distribution. Four cases were considered, *viz.*, a polydispersion with: (i) no droplet interactions; (ii) measured coalescence and breakage rates; (iii) "infinite" coalescence and breakage rates; and (iv) a monodispersion with droplets of diameter equal to the Sauter mean diameter of the polydispersion. The droplet interactions in case (ii) were allowed for by means of the stochastic procedure based on a Monte Carlo random selection method, used in step 7 of Hamilton and Pratt's computer program (1984).

The results of the computations, summarized in Table 8, indicate that the effect of polydispersivity itself, and hence of droplet coalescence and breakage, is surprisingly small for the pulsed column, unlike the packed column (Hamilton and Pratt, 1984). For practical design purposes, therefore, there is a welcome simplification in that the dispersed phase can be treated as a monodispersion of diameter equal to the Sauter mean diameter of the polydispersion.

## DISCUSSION

The derived values of the rate constants, plotted in Figures 5, 6(a)–(c) and 7(a)–(c), show considerably less scatter than was the case for the packed column (Hamilton and Pratt, 1984). This is undoubtedly due to the additional uncertainty resulting from the use of a random packing in the latter case. There is some tendency in the present work for the plots of rate constant against $d_j$ to be convex downwards, but this may well result from the truncation of the droplet-size distribution at the two ends.

TABLE 8. EFFECT OF DROPLET COALESCENCE AND BREAKAGE ON MASS TRANSFER PERFORMANCE

| Case | Without Backmixing $N_{od}$ | Without Backmixing $N^1_{od}$ | Without Backmixing No. of Stages* | With Backmixing $N_{od}$ | With Backmixing $N^1_{od}$ | With Backmixing No. of Stages* |
|---|---|---|---|---|---|---|
| (a) Pulse Frequency = 60 cycles/min | | | | | | |
| (i) No coalescence | 7.626 | 0.255 | 29.85 (1.002) | 10.436 | 0.254 | 41.10 (1.001) |
| (ii) Measured coalescence & breakage rates | 7.628 | 0.256 | 29.79 (1.000) | 10.444 | 0.254 | 41.07 (1.000) |
| (iii) Infinite coalescence | 7.680 | 0.269 | 28.59 (0.960) | 10.646 | 0.269 | 39.63 (0.965) |
| (iv) Monodispersion of size $d_{32}$ | 7.728 | 0.278 | 27.81 (0.934) | 10.780 | 0.278 | 38.79 (0.944) |
| (b) Pulse Frequency = 90 cycles/min (corresponds to emulsion operation) | | | | | | |
| (i) No coalescence | 8.211 | 0.378 | 21.71 (1.006) | 19.777 | 0.373 | 52.98 (1.004) |
| (ii) Measured coalescence & breakage rates | 8.223 | 0.381 | 21.57 (1.000) | 19.883 | 0.377 | 52.77 (1.000) |
| (iii) Infinite coalescence | 8.297 | 0.394 | 21.08 (0.977) | 20.439 | 0.394 | 51.92 (0.984) |
| (iv) Monodispersion of size $d_{32}$ | 8.371 | 0.412 | 20.30 (0.941) | 21.049 | 0.412 | 51.03 (0.967) |
| (c) Pulse Frequency = 120 cycles/min | | | | | | |
| (i) No coalescence | 8.607 | 0.459 | 18.77 (1.004) | 22.880 | 0.454 | 50.43 (1.002) |
| (ii) Measured coalescence & breakage rates | 8.620 | 0.461 | 18.69 (1.000) | 22.992 | 0.457 | 50.31 (1.000) |
| (iii) Infinite coalescence | 8.680 | 0.475 | 18.27 (0.978) | 23.595 | 0.475 | 49.69 (0.988) |
| (iv) Monodispersion of size $d_{32}$ | 8.617 | 0.463 | 18.60 (0.995) | 23.214 | 0.463 | 50.12 (0.996) |

* The bracketed values are the ratios of the numbers of stages required to those for Case (ii).

Although the rate constants are not strictly comparable numerically for the two types of column, or for the two types of operation with the present column, due to differences in dimensions, it is of interest that the effect of holdup was qualitatively similar in all cases. The coalescence constants decreased with increase in droplet size for both columns, although the effect was much greater for the pulsed column. On the other hand, the breakage constants were much less affected by droplet size in both cases, although the exponents on $d_j$ were of opposite sign.

The predicted effects of both polydispersivity and of droplet coalescence and breakage were surprisingly small, and were considerably less than for the packed column (Hamilton and Pratt, 1984). However, despite this, a knowledge of the rate constants is likely to be of considerable importance, both to design and to the interpretation of column test data. Thus it would enable not only the steady-state droplet-size distribution, and hence the interfacial area for mass transfer to be predicted, but also the change in these parameters as the size distribution of the droplets entering the column from the distributor approaches the steady state.

Before such methods could come into general use it would be necessary to know the effects of physical properties and column geometry on the rate constants. In the absence of data for other systems, the effect of the former could be predicted from the present data by dimensional analysis, as shown by Hamilton and Pratt (1984) for the packed column. Thus, the phase flow rates are already taken into account in Eq. 29 by the holdup, $x_d$. The most important remaining variables are the density difference, interfacial tension and gravitational acceleration, and dimensional analysis shows that these can be related, e.g., as follows

$$\phi_1(k_j) \text{ or } \phi_2(K_j) = a' \left(\frac{d_j^2 \Delta\rho g}{\gamma}\right)^{b'} x_d^{c'} \qquad (35)$$

where $\phi_1(k_j)$ and $\phi_2(K_j)$ are given by

$$\text{Mixer-settler operation: } \phi_1(k_j) = \frac{k_j^4 \Delta\rho^3 g}{\gamma^3};\ \phi_2(K_j) = \frac{K_j{}^4 \gamma}{\Delta\rho g^3}$$

$$\text{Emulsion operation: } \phi_1(k_j) = \frac{k_j^4 \Delta\rho^7 g^5}{\gamma^7};\ \phi_2(K_j) = \frac{K_j^4 \Delta\rho}{\gamma g}$$

Hence the values of $a'$, $b'$ and $c'$ in Eq. 35 can be estimated from the values of $a$, $b$ and $c$ given in Table 6.

## NOTATION

$a$ = pulse amplitude, i.e., total displacement of liquid in column, cm
$a_{i,j}$ = element in $i$th row and $j$th column of matrix **A** (Eq. 15)
$B$ = constant in Eq. 1
$b_1, b_2, b_3$ = constants in Eq. 2
$C_c$ = auxiliary variable defined by Eq. 34, g cm$^{-3}$
$c_c$ = solute concentration in continuous phase, g·cm$^{-3}$
$c_d$ = solute concentration in dispersed phase, g·cm$^{-3}$
$d_j$ = mean diameter of $j$th droplet size range, mm or cm
$d_o$ = mean diameter of smallest droplet size range, mm or cm
$d_{32}$ = Sauter mean diameter of droplets, mm or cm
$E$ = extraction factor, $U_c/mU_d$
$F_i(y)$ = $i$th element of column vector $\boldsymbol{F}(y)$ (Eq. 22)
$\boldsymbol{f}$ = column vector of $f_j$ values
$f$ = pulse frequency, min$^{-1}$ or s$^{-1}$
$f_j$ = number fraction of red droplets in size range $j$
$g$ = gravitational acceleration, cm·s$^{-2}$
$\boldsymbol{J}^k$ = Jacobian matrix at $k$th iteration
$K_{od}$ = overall dispersed-phase mass transfer coefficient, cm·s$^{-1}$
$K_j$ = first-order breakage rate constant for droplets of size $j$, s$^{-1}$ (mixer-settler operation), cm·s$^{-1}$ (emulsion operation)
$k_j$ = second-order coalescence rate constant for droplets of size $j$, cm$^2$·s$^{-1}$ (mixer-settler operation) cm$^4$·s$^{-1}$

(emulsion operation)

$k_j^{j-1}$ = second-order rate constant for coalescence of size $j$ with size $j-1$ droplets (dimensions as for $k_j$)

$L$ = stage height, cm

$M$ = number of droplet size intervals

$m$ = gradient of equilibrium line, $dc_d^*/dc_c$

$N$ = number of stages (i.e., plates)

$N_{od}$ = number of overall dispersed phase transfer units

$N_{od}^1$ = number of overall dispersed phase transfer units per actual stage

$n_j$ = number of droplets of size $j$ per unit plate area, $cm^{-2}$ (mixer-settler) or per unit column volume, $cm^{-3}$ (emulsion operation)

$p$ = fractional number of coalescences between droplets of size $j$ with $j-1$ which give droplets of size $j+1$

$Re_{d,j}$ = Reynolds number for droplets of size $j$, $d_j v_{r,j} \rho_c / \mu_c$

$s$ = $f$ (mixer-settler operation), $s^{-1}$, or $U_d/x_d$ (emulsion operation), $cm \cdot s^{-1}$

$t$ = time, s

$U_c, U_d$ = superficial velocity of continuous and dispersed phase respectively, $cm \cdot s^{-1}$

$V_c, V_d$ = volumetric flow rate of continuous and dispersed phase respectively, $cm^3 \cdot s^{-1}$

$\bar{v}_r$ = characteristic velocity, $cm \cdot s^{-1}$

$v_o, v_j$ = volume of droplet of sizes $o$ and $j$ respectively, $cm^3$

$v_{r,j}$ = relative velocity of droplets of size $j$, $cm \cdot s^{-1}$

$x_d$ = fractional holdup of dispersed phase

$x_j$ = $j$th element of column vector $x$ (Eq. 15)

$y_j$ = $j$th element of transformed column vector $y$ (Eq. 23)

$z_i$ = $i$th element of column vector z (Eq. 15)

### Greek Letters

$\alpha_c$ = backmixing ratio for continuous phase

$\Delta_j, \Delta_j^R$ = rate of change of number concentration of total and of red droplets respectively per unit cross-sectional area, $cm^{-2} \cdot s^{-1}$

$\epsilon_i$ = $i$th element of residual vector (Eq. 18)

$\Delta\rho$ = density difference between phases, $g \cdot cm^{-3}$

$\mu_c$ = viscosity of continuous phase, $g \cdot cm^{-1} \cdot s^{-1}$

$\rho_c$ = density of continuous phase, $g \cdot cm^{-3}$

$\gamma$ = interfacial tension between phases, $g \cdot s^{-2}$

### Subscripts

$c$ = continuous phase

$d$ = dispersed phase

$i,j$ = droplet size range

$n$ = plate number

in = dispersed phase entering

out = continuous phase leaving

### Superscripts

$f$ = flood point value

$k$ = iteration number

$T$ = transpose

$*$ = equilibrium value

$-$ = mean value over all droplets

### LITERATURE CITED


Barrodale, I., and F. D. K. Roberts, "An Improved Algorithm for Discrete $l_1$ Linear Approximation," *SIAM J. Num. Anal.*, **10**, p. 839 (1973).

Barrodale, I., and F. D. K. Roberts, "Solution of an Overdetermined System of Equations in the $l_1$ Norm," *Comm. of the A.C.M.*, **17**, p. 319 (1974).

Carnahan, B., H. A. Luther, and J. O. Wilkes, *Applied Numerical Methods*, Chapter 5, John Wiley (1969).

Coulaloglou, C. A., and L. L. Tavlarides, "Description of Interaction Processes in Agitated Liquid-Liquid Dispersions," *Chem. Eng. Sci.*, **32**, p. 1289 (1977).

Curtis, A. R., *Optimization in Action*, Ed., L. C. W. Dixon, Academic Press, London (1976).

Garg, M. O., "Measurement and Modelling of Droplet Coalescence and Breakage in a Pulsed Plate Liquid Extraction Column," Ph.D. Thesis, University of Melbourne (1982).

Garg, M. O., and H. R. C. Pratt, "Effect of Column Diameter on Backmixing in Pulsed Plate Columns," *I.E.C. Proc. Des. Dev.*, **20**, p. 492 (1981).

Griffith, R. M., "Mass Transfer from Drops and Bubbles," *Chem. Eng. Sci.*, **12**, p. 198 (1960).

Hamilton, J. A., "Droplet Coalescence and Breakage in a Packed Liquid Extraction Column," Ph.D. Thesis, University of Melbourne (1981).

Hamilton, J. A., and H. R. C. Pratt, "Measurement of Droplet Coalescence Rates in a Packed Extraction Column Using a Novel Colorimetric Technique," *Proc. Int. Solv. Extn. Conf.*, Paper No. 80-19 (1980).

Hamilton, J. A., and H. R. C. Pratt, "Droplet Coalescence and Breakage Rates in a Packed Liquid Extraction Column," *AIChE J.* p. 442 (1984).

Marquardt, D. W., "An Algorithm for Least Squares Estimation of Nonlinear Parameters," *SIAM J. Appl. Maths.*, **11**, p. 431 (1963).

Ramshaw, C., and J. D. Thornton, "Droplet Breakdown in a Packed Liquid Extraction Column," *I. Chem. E. Symp. Ser.*, No. 26, *Liquid-Liquid Extraction*, 73 (1967).

Rice, J. R., *The Approximation of Functions*, **1**, p. 20, Addison-Wesley Pub. Co., Reading, MA (1964).

Rouyer, H., J. Lebouhellec, E. Henry, and P. Michel, "Present Study and Development of Extraction Pulsed Columns," *Proc. Int. Solv. Ext'n. Conf.*, **3**, p. 2339 (1974).

Rozen, A. M., and A. I. Bezzubova, "Mass Transfer in Individual Drops," *Foundations Chem. Eng. (Consultants Bureau Trans.)*, **2**, p. 715 (1968).

Sege, G., and F. W. Woodfield, "Pulsed Column Variables," *Chem. Eng. Prog.*, **50**, p. 396 (1954).

Thornton, J. D., "Liquid-Liquid Extraction, Part XIII: The Effect of Pulse Wave Form and Plate Geometry on the Performance and Throughput of a Pulsed Column," *Trans. Inst. Chem. Eng.*, **35**, p. 316 (1957).

Thorsen, G., and S. G. Terjesen, "On the Mechanism of Mass Transfer in Liquid-Liquid Extraction," *Chem. Eng. Sci.*, **17**, p. 137 (1962).

Van De Panne, C., "Methods for Linear and Quadratic Programming," North Holland Pub. Co., Amsterdam (1975).

Vermijs, H. J. A., and H. Kramers, "Liquid-Liquid Extraction in a Rotating Disc Contactor," *Chem. Eng. Sci.*, **3**, p. 55 (1954).


*Supplementary material has been deposited as Document No. 04177 with the National Auxiliary Publications Service (NAPS), c/o Microfiche Publications, 214-13 Jamaica Avenue, Queens Village, N.Y. 11428, and may be obtained for $4.00 for microfiche or $7.75 for photocopies.*


*Manuscript received July 9, 1982; revision received April 18, and accepted May 10, 1983.*